Composites: Part A 143 (2021) 106311

Contents lists available at ScienceDirect

Composites Part A

journal homepage: www.elsevier.com/locate/compositesa

Theoretical prediction of effective stiffness of nonwoven fibrous networks with straight and curved nanofibers

Mang Zhang [a], Wenbin Lu [b], Pelagia Irene Gouma [c], Zhiping Xu [d], Lifeng Wang [a,*]

[a] Department of Mechanical Engineering, State University of New York at Stony Brook, Stony Brook, NY 11794, USA
[b] Department of Applied Mathematics and Statistics, State University of New York at Stony Brook, Stony Brook, NY 11794, USA
[c] Department of Materials Science and Engineering, The Ohio State University, Columbus, OH 43210, USA
[d] Department of Engineering Mechanics, Tsinghua University, Beijing 100084, China

ARTICLE INFO

Keywords:
Nonwoven network
Crosslink rotation
Fiber curvature
Stiffness

ABSTRACT

The nonwoven random fibrous network materials have been widely used in many fields due to their excellent physical and chemical properties. To understand the mechanical behavior of these nonwoven fibrous networks, a theoretical model is developed based on the network microstructure and microstructure evolution in the loading process. It is revealed that the effective stiffness of nonwoven fibrous networks is not only contributed by the fiber stretching and bending, but also depending on the rotation deformation of crosslinks between fibers. Since the nonwoven fibrous networks are constructed by straight or curved fibers, especially at nanoscale, the curvature effects on the effective stiffness are also studied systematically. Furthermore, finite element simulation is conducted to verify the theoretical predictions on the elastic properties of nonwoven fibrous networks consisting of straight and curved fibers, respectively. The theoretical model presented here is a general model, enabling to capture the elastic mechanical behavior of many complex nonwoven network systems from micro to nano length scales.

1. Introduction

The nonwoven fibrous networks constructed by randomly distributed fibers are widely observed in natural and synthetic materials at different length scales, including silkworm cocoon, extracellular tissues [1,2], metal nanowire networks [3,4], carbon nanotube films [5–7], and electrospun polymer fiber mats [8,9]. Due to their unique properties, nonwoven fibrous network materials have attracted much attention for many applications. Since these materials are highly porous, the mechanical property is clearly the first task to be investigated. Experiments have been performed to reveal the fundamental mechanics of nonwoven networks. For example, an X-ray phase contrast imaging is used to capture the local fibers deformation under a tensile loading test, showing microstructure evolutions of fiber stretching, fiber bending, and the crosslink rotation [10,11]. Computational models are also established to study the nonwoven network mechanical behaviors extensively. It is found that the geometrical parameters have significant influences on the network's mechanical properties [12–16], which include the network volume fraction, the fiber aspect ratio (ratio of fiber length and fiber diameter), and the fiber curvature [12,17–19]. Besides, a lot of efforts have been made to understand the relationship between the network microstructure and its macroscopic mechanical response [13,20–22]. Nonwoven networks with higher volume fraction, larger fiber aspect ratio, and smaller fiber curvature are normally stiffer and stronger. Although the effect of network volume fraction and fiber aspect ratio has been well studied, the deformation mechanism of the nonwoven networks with curved fibers, which is most likely true at nanoscale, remains largely unexplored [23,24].

Recently, Pai *et al.* have introduced a stiffness ratio to express the curvature effect on the network Young's modulus, which is the ratio of the curved fiber network Young's modulus and the straight fiber network Young's modulus [25]. In their research, a represented volume element (RVE) model with four fibers interacting at the same point has been built. The stiffness ratio has been found to depend on the fiber curvature and the average segment length in the network. Another theoretical model has been developed based on a bilayer of triangular truss network structure, which has six or more fibers interacting at the same point [26]. It describes the network's microstructural evolution and macro elastic–plastic behavior with large deformation. However, from their scanning electron microscope images, only two fibers are

* Corresponding author.
E-mail address: Lifeng.wang@stonybrook.edu (L. Wang).

https://doi.org/10.1016/j.compositesa.2021.106311
Received 14 April 2020; Received in revised form 23 September 2020; Accepted 28 January 2021
Available online 2 February 2021

observed to interact at the same point. Apart from the numerical and theoretical studies with RVE models, a simple cantilever beam model has been created to investigate the stiffness of nonwoven networks with straight fibers [27]. In this model, the effective network Young's modulus is described as the average Young's modulus of segments in all orientations. In this way, the random distribution nature of all fibers is well expressed. The average segment length is considered as the beam length, which corresponds to the network volume fraction and covers the network topological properties. However, the network stiffness prediction using this model is larger than those obtained from the experimental measurements, given that only fiber stretching deformation is considered. Clearly, the bending deformation of fibers also plays a significant role during macroscopic deformation of the nonwoven networks. Besides the bending, another important parameter that influences the network stiffness is the fiber crosslink stiffness. To identify the crosslinks and the projected intersections, 2.5D and 3D models have been developed for multiple layers of networks, and only the fibers that are close enough to each other in the thickness direction are considered to count as a crosslink [28–30]. Another way to identify the crosslink number is to adjust the percentage of the effective cross links from experiments to simulations [31,32]. In all those works, the crosslink is considered as two types, either rigid connected or not connected. A model for a flexible connection is still in need. Besides, the crosslink properties for the carbon nanotube network is found to be related to the binder properties and can lead to very different network behaviors [5]. Therefore, it is urgent to develop a theoretical model which can reflect the crosslink conditions of the nonwoven networks.

In this study, we develop theoretical models for the mechanics of nonwoven networks constructed by straight fibers or curved fibers, where the local fiber bending and crosslink rotation are also considered. A rotating crosslink model (RCLM) is built to investigate the effective stiffness of nonwoven fiber networks. Parametric studies are performed to study the effects of crosslink rotational stiffness and fiber curvature on the macroscopic properties. Moreover, a representative volume element based finite element model with long fibers is used to validate the theoretical predictions.

2. Theoretical model for the elastic property of nonwoven fibrous networks

For the nonwoven network constructed by randomly distributed fibers, the network local deformations under tension are found to involve fiber stretching, fiber bending, and crosslink rotation (Fig. 1(a)) [13]. To capture all of these, a RCLM is developed on a single fiber segment with a rotational crosslink for straight fiber networks and curved fiber networks, respectively (Fig. 1(b–c)). Considering the random distribution of fiber orientations in the network, the macroscopic effective Young's modulus can be expressed as

$$E_n = \frac{\int_0^{\frac{\pi}{2}} E_e(\alpha) d\alpha}{\int_0^{\frac{\pi}{2}} d\alpha} \tag{1}$$

where α is the angle between a fiber segment orientation and the horizontal direction, and $E_e(\alpha)$ is the equivalent Young's modulus of the fiber segment [15].

2.1. RCLM for network with straight fibers

In the random nonwoven network consisting of straight fibers, a RCLM is built based on a straight beam segment with a loading force F applied on the right end, and the left end is rotationable with a rotational stiffness k_c (Fig. 1(b)). The length of the beam is the average segment length l_c in the network. Considering the network as a 2D one-layer material, the network thickness is the same as the fiber diameter. The fiber length per unit area can be calculated as $\rho = NL/L_1L_2$, where L_1 and L_2 are the length and width of the network domain area, N is the number of fibers in the network domain area, and L is the average length of a single fiber. According to the Corte-Kallmes theory [33], $l_c = \pi/2\rho$. Then l_c here can be expressed as

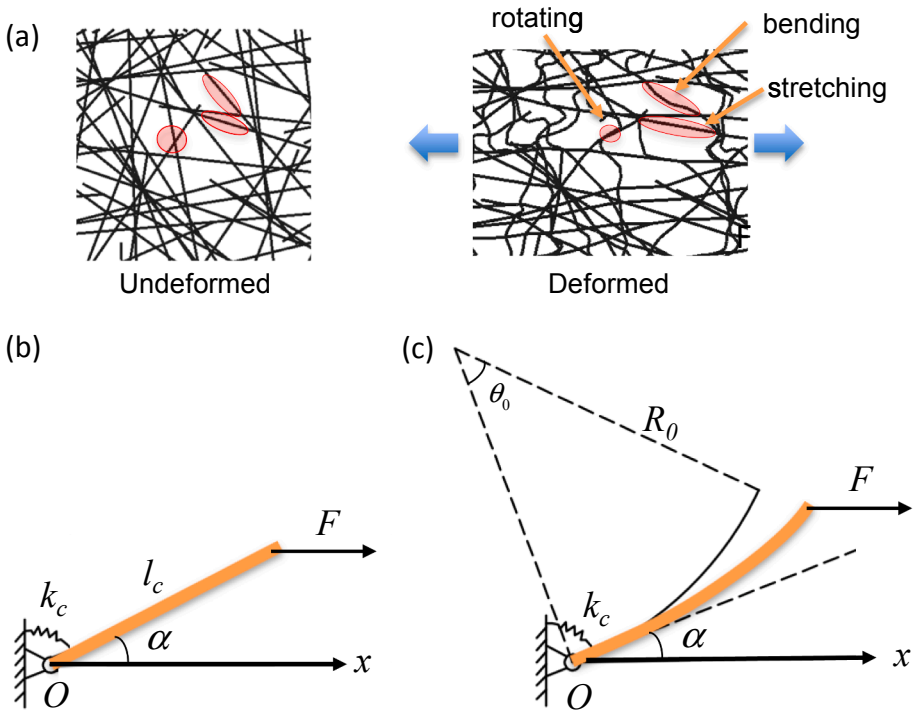

Fig. 1. (a) The deformation of a nonwoven random network under uniaxial tension, where fiber stretching, fiber bending, and crosslink rotation are observed. (b) Rotating crosslink model with a straight fiber. (c) Rotating crosslink model with a curved fiber. (For interpretation of the references to colour in this figure legend, the reader is referred to the web version of this article.)

$$l_c = \pi L_1 L_2 / 2NL. \tag{2}$$

The moment due to the applied force can be expressed as

$$M = Fsin(\alpha) l_c = k_c \cdot \beta, \tag{3}$$

where β is the corresponding rotation angle of the beam about origin O. The axial stretching displacement of the beam can be obtained as

$$\Delta l = \frac{Fcos(\alpha) l_c}{E_f A}, \tag{4}$$

where E_f is the Young's modulus of a single fiber, and A is the fiber cross section area. The deflection of the beam is defined by the Euler beam theory, and the deflection of the right end of the beam can be calculated as

$$w(l_c) = \frac{Fsin(\alpha) l_c^3}{3E_f I} + \beta l_c, \tag{5}$$

where I is the moment of inertia. Therefore, the displacement of the loading end along the x direction can be expressed as

$$u_x = \Delta l cos(\alpha) + w(l_c) sin(\alpha). \tag{6}$$

And the equivalent Young's modulus of the segment with a given orientation α can be obtained as

$$E_e(\alpha) = \frac{F \cdot l_c cos(\alpha)}{u_x \cdot A / cos(\alpha)}. \tag{7}$$

Then, applying a small loading force, the effective network Young's modulus can be obtained via Eq. (1).

2.2. RCLM for network with curved fibers

Due to large aspect ratio, microfibers and nanofibers are easily seen to have curvatures under many constraints during the fabrication and manufacturing process. The RCLM considering curved fiber networks is indicated in Fig. 1(c). The curved beam model here is in an arc shape with its length of l_c and the initial radius of R_0. Then the initial center angle of the fiber segment is $\theta_0 = l_c / R_0$. At a distance of s from the fixed end, the bending moment applied on the beam is [34]

$$M = F[y(l_c) - y(s)]. \tag{8}$$

The rotation angle can be solved via

$$M = \beta \cdot k_c = F \cdot 2R_0 sin\left(\frac{\theta}{2}\right) \cdot sin\left(\alpha + \frac{\theta}{2}\right), \tag{9}$$

where θ is the current center angle of the fiber segment. And the curvature of the beam can be given as

$$\frac{d\theta}{ds} = \frac{1}{R_0} - \frac{F[y(l_c) - y(s)]}{E_f I}. \tag{10}$$

Taking into account of the geometrical relation

$$\frac{dy}{ds} = sin(\alpha - \beta + \theta), \tag{11}$$

Eq. (10) can be differentiated with respect to s as

$$\frac{d^2\theta}{d^2 s} = \frac{F}{E_f I} \frac{dy}{ds} = \frac{F}{E_f I} sin(\alpha - \beta + \theta). \tag{12}$$

Set θ_d as the center angle of the deformed curved beam segment, after integrating, the curvature can be expressed as

$$\frac{d\theta}{ds} = \sqrt{\frac{1}{R_0^2} - \frac{2F}{E_f I}[cos(\alpha - \beta + \theta) - cos(\alpha - \beta + \theta_d)]}. \tag{13}$$

Considering the beam here is also extensible, the differential normal extension is

$$ds = [1 + \frac{F}{E_f A} cos(\alpha - \beta + \theta)] ds_0. \tag{14}$$

Then the initial length of the curved beam l_c can be expressed as

$$l_c = \int_0^{l_c} ds_0 = \int_0^{l_c} \frac{1}{1 + \frac{F}{E_f A} cos(\alpha - \beta + \theta)} ds. \tag{15}$$

Substituting Eq. (13), it shows

$$l_c = \int_0^{\theta_d} \frac{1}{1 + \frac{F}{E_f A} cos(\alpha - \beta + \theta)} \frac{1}{\sqrt{\frac{1}{R_0^2} - \frac{2F}{E_f I}[cos(\alpha - \beta + \theta) - cos(\alpha - \beta + \theta_d)]}} d\theta. \tag{16}$$

Given the value of α, the deformed center angle θ_d can be solved numerically. Note that the displacement of the loading end in the $\times$ direction is

$$u_x = x(l) - x(l_0), \tag{17}$$

where $x(l)$ is the horizontal coordinate of the deformed beam end, which is given by

$$x(l) = \int_0^l cos(\alpha - \beta + \theta) \cdot ds = \int_0^{\theta_d} \frac{cos(\alpha - \beta + \theta)}{\sqrt{\frac{1}{R_0^2} - \frac{2F}{E_f I}[cos(\alpha - \beta + \theta) - cos(\alpha - \beta + \theta_d)]}} d\theta. \tag{18}$$

$x(l_0)$ is the horizontal coordinate of the initial beam end,

$$x(l_0) = 2R_0 sin(\frac{\theta}{2}) cos(\alpha + \frac{\theta}{2}). \tag{19}$$

Therefore, the equivalent Young's modulus of the segment with orientation of α can be expressed as

$$E_e(\alpha) = \frac{F \cdot x(l_0)}{u_x \cdot A / cos(\alpha)}. \tag{20}$$

Then the effective Young's modulus for the whole network can be solved numerically with Eq. (1). Note that because the beam shape is no longer symmetric about its original axial direction, a larger integration range, $[-\frac{\theta_0}{2} - \frac{\pi}{2}, -\frac{\theta_0}{2} + \frac{\pi}{2}]$, for α should be used.

For networks with curved fibers, the l_c evaluation is different from that for networks with straight fibers. For networks with straight fibers, two interacted fibers only have one interaction point, while one or two interaction points are possible for two interacted fibers in networks with curved fibers. It is expected that the connection between fibers with two interaction points is enhanced. However, the connection between the local fiber to the overall network is cut down [18]. Therefore, the average segment length should be adjusted in networks with curved fibers.

To solve the average segment length of curved fibers, the probability of two arcs interacting P needs to be evaluated. From the geometry, the first step is to solve the interacting probability of two circles, and the second step is to solve the arcs interacting probability in these two circles. Assuming these two arcs have same length and curvature, the two circles containing these two arcs have the same radius of R, as shown in Fig. 2 (a). Given a solid-line circle in a domain area of $L_1 \times L_2$, the dash-line circle can interact with the solid-line circle when the center point of the dash-line circle locates within the orange area, which is a circle with a radius of $2R$. The probability of two circles intersecting is

$$P_1 = \frac{\pi \cdot (2R)^2}{L_1 L_2}. \tag{21}$$

If θ_a is the center angle of the arc and θ_{in} is the center angle of the intersection part of two circles, there will be two cases to evaluate the arcs intersecting conditions: (a) $\theta_a < \theta_{in}$, and there exists only one

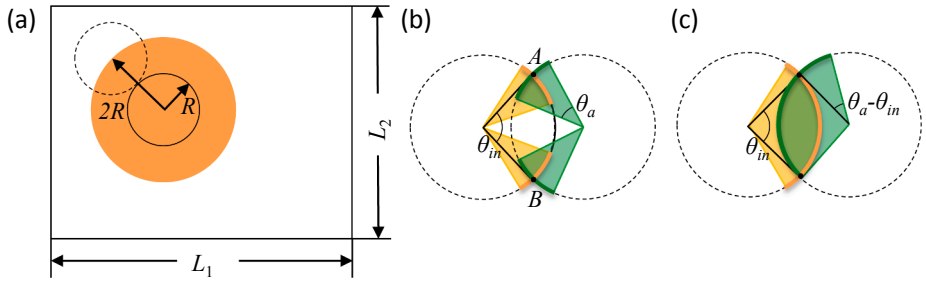

Fig. 2. Schematic diagram of the probability of two arcs in-plane interacting with each other. (a) Domain area, (b) case $\theta_a < \theta_{in}$, and (c) case $\theta_a \geqslant \theta_{in}$. (For interpretation of the references to colour in this figure legend, the reader is referred to the web version of this article.)

intersection, b) $\theta_a \geqslant \theta_{in}$, there exist one or two intersections. For case (a) (Fig. 2(b)), two arcs can interact at either point A or point B. The probability for two arc intersecting is

$$P_{2a} = 2\left(\frac{\theta_a}{2\pi}\right)^2. \tag{22}$$

For case (b) (Fig. 2(c)), the two points interacting is over counting, comparing with case (a). And the adjusted probability for two arc interacting is

$$P_{2b} = 2\left(\frac{\theta_a}{2\pi}\right)^2 - \left(\frac{\theta_a - \theta_{in}}{2\pi}\right)^2. \tag{23}$$

The expectation of the distance between the centers of these two interacting circles is

$$\bar{l} = \frac{\int_0^{2\pi}\int_0^{2R} 2R \cdot dtd\theta}{\int_0^{2\pi} 2R \cdot d\theta} = R. \tag{24}$$

Clearly, the expectation for θ_{in} is $\pi/3$. Therefore, the probability of two are interacting can be expressed as

$$P = \begin{cases} P_1 P_{2a} & (\theta_a < \pi/3); \\ P_1 P_{2b} & (\theta_a \geqslant \pi/3). \end{cases} \tag{25}$$

Since the number of crosslinks on one fiber is NP, the average segment length can be calculated as $l_c = L/(NP+1)$.

3. Finite element method simulation

Finite element (FE) simulations are introduced to verify the theoretical results, with a representative volume element (RVE) model [13]. In the model, fibers with the same length and diameter are initially built with a uniform distribution in a plane with ABAQUS scripting via Python. All fibers are firstly generated with their middle point on the center of the RVE area, and then each fiber is rotated and transported by a random angle and a random vector, respectively. Finally, the fiber segments beyond the RVE boundary are cut and moved back to the opposite inside. In this way, a network with random fiber orientation and distribution is generated. The FE simulations are conducted via a commercial finite element package ABAQUS/Explicit quasi-static method (Simulia, Provindence, RI). Strain controlled periodic boundary conditions (PBCs) are applied to the surface of RVE, and the RVE deforms in a periodically repeating manner without any overlaps or cavities.

To gain the averaged results in the FE simulations, five networks with same network density and curvature are simulated. In both theoretical predictions and the FE simulations, the material property of fiber is considered as fiber Young's modulus of $E_f = 4100$ MPa, Poison's ratio of $\nu = 0.4$. Considering the effective/average property is under study, to simplify the problem, all fibers have the same length and same diameter, and curved fibers have the same curvature radius.

4. Results and discussions

4.1. Effective stiffness of nonwoven networks with straight fibers

Fig. 3(a) shows normalized Young's modulus (E_n/E_f) of nonwoven fiber networks with fiber volume fraction from 0.05 to 0.25, where different model predictions, FE simulation results, and experimental results are compared. It's clear that normalized network Young's modulus increases as the fiber volume fraction increases, which is captured by all theoretical models. A simplified analytical model that neglects the bending deformation of fibers always over predicts the results than experiments and simulations (see Yin *et al.* [27]). If the bending deformation of fibers is considered, the prediction is significantly smaller, as shown by the red solid line of current RCLM with $k_{c1} = \infty$. This means the rotational stiffness of crosslinks is infinite, and in other words, only fiber bending and stretching are considered. Since this is still over constrained, this red line predicted by the RCLM presents larger estimations of the network stiffness than the results from simulations and experiments. It also indicates that besides the bending and the stretching deformation, there is another deformation mechanism, which is the crosslink rotation that observed in the microstructure, having unneglectable contribution to the network effective stiffness. Such intrinsic degree of freedom is presented by the rotational spring in the RCLM. By adjusting k_c, it is possible to accurately predict the network stiffness obtained by simulations and experiments. For example, when $k_c = 1.3 \times 10^{-5}$Nμm/rad, the effective stiffness the PA6 network measured from the tensile experiment [26] can be captured precisely, as shown in Fig. 3(a). Two curves with larger k_c are also plotted to provide better estimations for experimental measurements of networks with larger fiber volume fraction. Note that the value of rotational stiffness k_c of crosslinks is determined by the connection of the joints between fibers during the material fabrication process. As $k_c$increases, the network stiffness can be enhanced dramatically, which is consistent with the molecular dynamic study on the improvement of the carbon nanotube network stiffness [5]. In FE simulations, rigid connections are assumed for all crosslinks between fibers, indicating the simulation results are the upper bound of experimental measurements. This is also clearly demonstrated in Fig. 3(a), where FE simulation results are larger than experimental data points at the same fiber volume fraction. Another reason leading to the difference between experimental results and simulation results is that fibers in the FE model are assumed to have uniform length and diameter. However, in the realistic experimental samples fiber length and diameter will vary based on different fabrication conditions and processes. Here, the FE model only presents the average value of these geometric parameters.

To have a better understanding how the k_c influences the network effective stiffness, the normalized network Young's modulus as a function of k_c is plotted in Fig. 4(a) for three different fiber volume fractions. When k_c is small, the network is hardly to carry any load because rotation leads to deformation easily. When k_c is larger, the network stiffness can be enhanced dramatically until approaching the dashed lines, corresponding to the cases where no crosslink rotation is allowed,

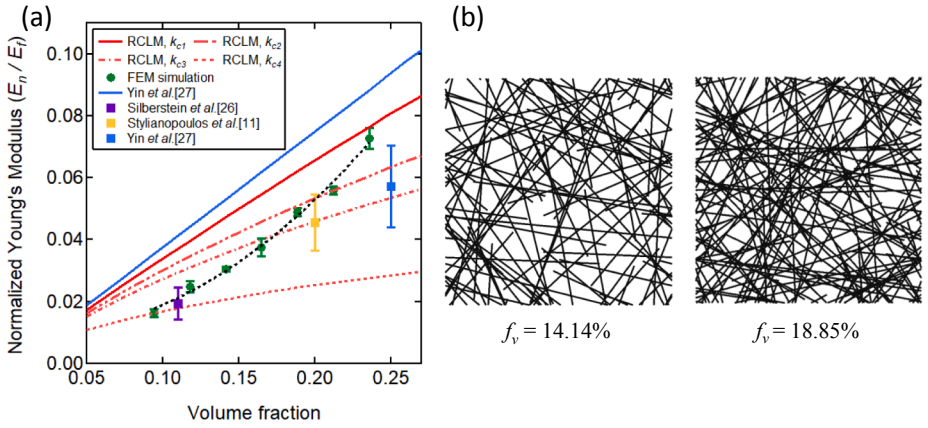

Fig. 3. (a) The normalized effective stiffness of fiber networks as a function of fiber volume fraction: $k_{c1} = \infty$, $k_{c2} = 3.1 \times 10^{-4}N\mu$m/rad, $k_{c3} = 1.5 \times 10^{-4}N\mu$m/rad, and $k_{c4} = 1.3 \times 10^{-5}N\mu$m/rad. (b) 2 representative nonwoven fiber networks with different fiber volume fractions. (For interpretation of the references to colour in this figure legend, the reader is referred to the web version of this article.)

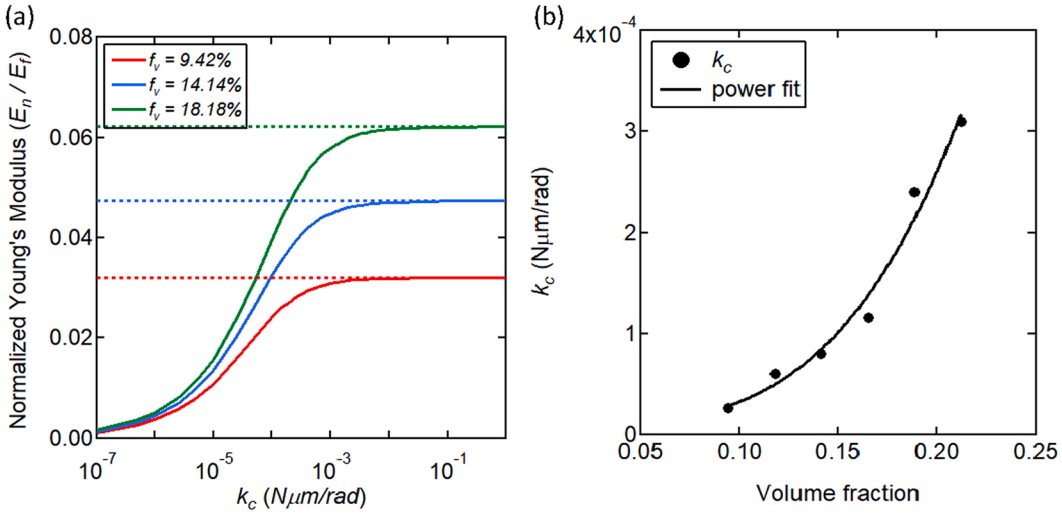

Fig. 4. (a) The network normalized Young's modulus as a function of k_c for networks with volume fractions of 9.42%, 14.14%, and 18.85%. (b) The rotational stiffness k_c as a function of fiber volume fraction in RCLM prediction. (For interpretation of the references to colour in this figure legend, the reader is referred to the web version of this article.)

i.e. $k_c \to \infty$. This result indicates that when $k_c$is larger than certain values (10^{-2}Nμm/rad here), enhancing the rotational stiffness of crosslinks won't be able to improve the effective network Young's modulus.

The rotational stiffness of crosslinks can also be affected by the fiber volume fraction in the network. It's clear that larger volume fraction or denser material distribution will limit the rotation of crosslinks and provide more resistance because of the shorter average segments (see Fig. 3(b)). Therefore, a larger rotational stiffness k_c is needed to predict the effective network stiffness when the fiber volume fraction is increased. To quantitatively show the relationship between k_c and f_v, a power function is used to fit the simulation results as

$$k_c = C_1 + C_2 \cdot f_v^{C_3} \tag{26}$$

with $C_1 = 1.07 \times 10^{-5}N\mu$m/rad, $C_2 = 7.13 \times 10^{-2}N\mu$m/rad, and $C_3 = 3.51$ respectively. This result agrees well with the FE simulation as shown in Fig. 4(b).

All these results indicate that introducing the fiber bending and crosslink rotating in the theoretical model can provide better estimations of the effective network stiffness of nonwoven random network structures, which is consistent with the deformation mechanisms observed in microstructure evolution under loading conditions. It should be noted that the accurate value of rotational stiffness of crosslinks is hard to be determined through experimental tests. More structure characterization might be needed for the experimental samples. It is expected the theoretical model presented here can be extended as a universal theoretical model that can be applied to other types of networks and cellular materials.

4.2. *Effective stiffness of nonwoven networks with curved fibers*

Fig. 5 shows the contours of RCLM predictions of network normalized Young's modulus for fiber volume fraction f_v varying from 9.42% to 18.85% at a given k_c, and the fiber center angle L/R_0 varies from 0.4 to 3. It is clear that the network stiffness always increases as f_v increases, which is consistent with FE simulation results. However, the L/R_0 effect is not significant until its value is larger than $\pi/3$. When the center angle is larger, the normalized Young's modulus decreases as the center angle increases.

The predictions from our RCLM are compared with results from a theoretical model of Pai *et al.* [25] and FE simulations. In both theoretical models, the normalized network Young's modulus is only dependent on the fiber volume fraction and the fiber center angle. Fig. 6 presents the comparison of different modulus predictions for the case

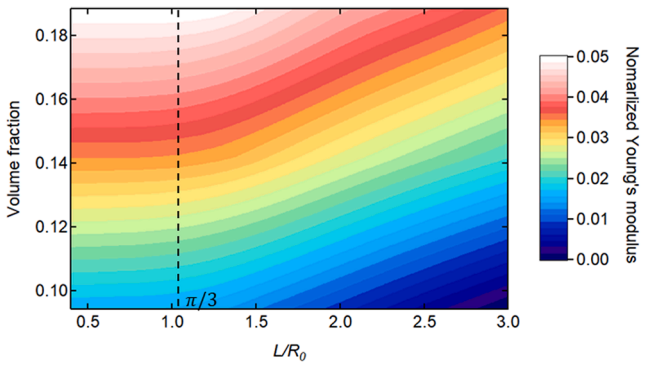

Fig. 5. The normalized Young's modulus of the nonwoven network as a function of f_v and L/R_0 when $k_c = 1.5 \times 10^{-4}$Nμm/rad. (For interpretation of the references to colour in this figure legend, the reader is referred to the web version of this article.)

that the fiber volume fraction is 18.85% and $k_c = 2.14 \times 10^{-5}N\mu$m/rad. To have a better understanding of the fiber curvature effect, a stiffness ratio is introduced here, which is the ratio of the curved fiber network stiffness and the straight fiber network stiffness. Clearly, when$L/R_0 \leqslant \pi/3$, the stiffness ratio predictions are almost the same and equals to ~1. This indicates that the theoretical models with straight fibers are applicable to networks with slightly curved fibers. However, the stiffness ratio predicted from both models starts to decrease dramatically when $L/R_0 > \pi/3$, which is consistent with FE simulation results. When $L/R_0 = 2.0$, the effective network stiffness is reduced up to 15% in this case. Note that the RCLM is more sensitive to the fiber curvature, giving a smaller stiffness ratio at a largerL/R_0, providing better estimation as compared to FE simulation results.

In the theoretical model of Pai *et al.* [25], four fibers interact at one crosslink, while practically there are only two fibers interacting at same joints in most cases. This will introduce extra constraints on the fibers and limit the fiber reorientation under loading, leading to a higher stiffness prediction. Moreover, the model introduces the curved fiber in an antisymmetric way, and two ending points and the middle point of the fiber are always on the same line, which can reduce the deflection of the beam structure, and further reduce the curvature effect. Note that RCLM predictions are closer to the FE simulation results, but still larger. Considering two end segments of any fiber in the FE model are free of loading and do not contribute to load carrying, it is reasonable to see RCLM overestimates the stiffness a bit in which all the fiber segments are assumed to be effective.

Fig. 7 shows the RCLM results on the effect of crosslink rotational stiffness $k_c$on the normalized Young's modulus of nonwoven fibrous networks consisting of curved fibers. Similar to the case of straight fibers, as k_c increases, the normalized Young's modulus increases up to a steady value when $k_c > 10^{-2}$Nμm/rad. When the curvatures of fibers are different, all results demonstrate a similar trend. Clearly, k_c is one of the most important parameters that dominate the effective stiffness of the nonwoven networks. Here, two volume fractions, $f_v = 9.42\%$ and $f_v = 18.85\%$ are also compared. If the stiffness ratio is calculated for different curvatures, it is found that the stiffness ratio for networks with lower volume fraction is more sensitive to the fiber curvature. Because lower volume fraction in the network results in greater average segment length, to increase the fiber curvature will more likely weaken the connections between fiber segments, leading to a weaker response of the network. This also indicates that k_c is smaller for the network where fibers are severely curved.

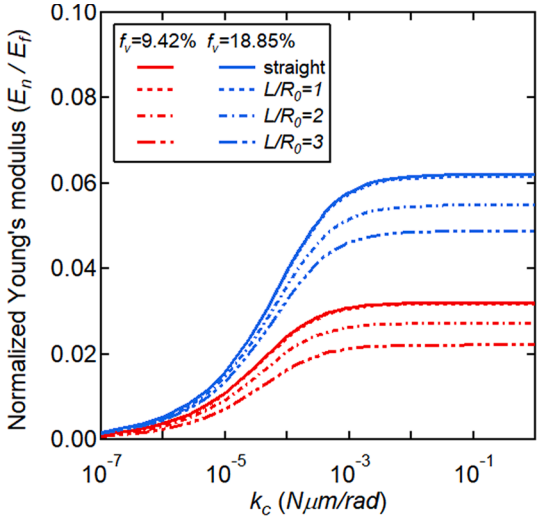

Fig. 7. RCLM prediction of the effect of crosslink rotational stiffness on the normalized Young's modulus of nonwoven fibrous networks consisting of straight fibers or curved fibers. Volume fractions of 9.42% and 18.85% are considered. (For interpretation of the references to colour in this figure legend, the reader is referred to the web version of this article.)

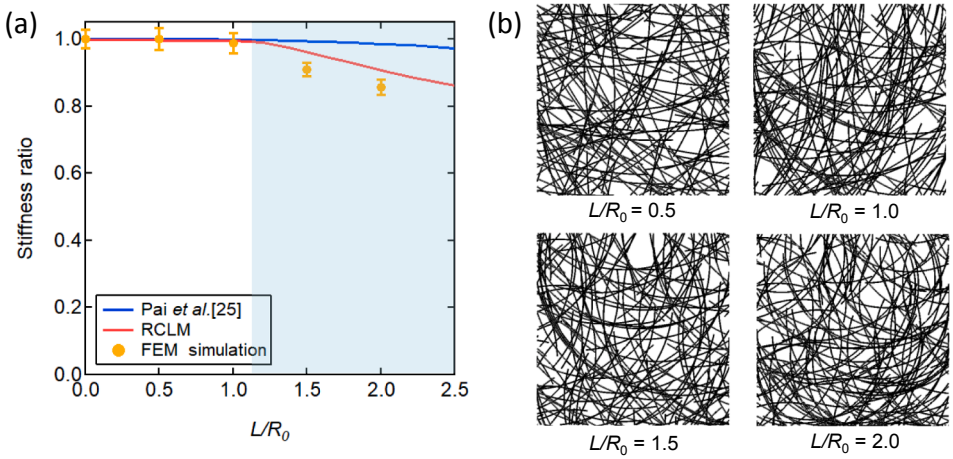

Fig. 6. The curvature effect on the network normalized Young's modulus. (a) The stiffness ratio comparing the results from RCLM model, model by Pai *et al.* [25], and FE simulations. (b) The corresponding nonwoven fiber networks with different L/R_0 in FE simulations. (For interpretation of the references to colour in this figure legend, the reader is referred to the web version of this article.)

5. Conclusions

In summary, to make a comprehensive understanding on the effective stiffness of random nonwoven fibrous networks consisting of straight fibers or curved fibers, a theoretical model based on beam theory and network microstructure (RCLM) is developed. It is revealed that the fiber stretching, fiber bending, and crosslink rotation deformation can significantly affect the effective mechanical response of nonwoven fibrous networks. It also suggests that enhancing the rotational stiffness of crosslinks between fibers is an effective way to improve the mechanical properties of nonwoven fibrous networks. Furthermore, the RCLM shows that when the fiber center angle is smaller than $\pi/3$, the fiber curvature has a negligible effect on the effective stiffness of the network. However, when the center angle is larger than $\pi/3$, the network stiffness can be reduced dramatically. These results are validated by the FE simulations. The model presented here provides a solid theoretical foundation for the design, optimization, and property prediction of randomly distributed nonwoven fibrous networks. However, there are still unrevealed factors, such as the strength of crosslinks and van der Waals interactions, that are not considered in this work and will be highlighted in our future work.

CRediT authorship contribution statement

Mang Zhang: Conceptualization, Methodology, Investigation, Formal analysis, Visualization, Writing - original draft. **Wenbin Lu:** Methodology, Formal analysis. **Pelagia Irene Gouma:** Conceptualization, Supervision, Writing - review & editing. **Zhiping Xu:** Conceptualization, Methodology, Writing - review & editing. **Lifeng Wang:** Conceptualization, Methodology, Investigation, Supervision, Validation, Writing - review & editing.

Declaration of Competing Interest

The authors declare that they have no known competing financial interests or personal relationships that could have appeared to influence the work reported in this paper.

Acknowledgements

The authors gratefully acknowledge the partial financial support from the National Science Foundation (CMMI-1724342).

References

[1] Chen FJ, Porter D, Vollrath F. Morphology and structure of silkworm cocoons. Mat Sci Eng C-Mater 2012;32(4):772–8.
[2] Camelliti P, Borg TK, Kohl P. Structural and functional characterisation of cardiac fibroblasts. Cardiovasc Res 2005;65(1):40–51.
[3] Ye S, Rathmell AR, Chen Z, Stewart IE, Wiley BJ. Metal nanowire networks: the next generation of transparent conductors. Adv Mater 2014;26(39):6670–87.
[4] Guo CF, Ren Z. Flexible transparent conductors based on metal nanowire networks. Mater Today 2015;18(3):143–54.
[5] Wang C, Wang L, Xu Z. Enhanced mechanical properties of carbon nanotube networks by mobile and discrete binders. Carbon 2013;64:237–44.
[6] Pan F, Chen Y, Liu Y, Guo Z. Out-of-plane bending of carbon nanotube films. Int J Solids Struct 2017;106:183–99.
[7] Yang HY, Han ZJ, Yu SF, Pey KL, Ostrikov K, Karnik R. Carbon nanotube membranes with ultrahigh specific adsorption capacity for water desalination and purification. Nat Commun 2013;4(1):1–8.
[8] Domaschke S, Morel A, Fortunato G, Ehret AE. Random auxetics from buckling fibre networks. Nat Commun 2019;10(1):1–8.
[9] Dorati R, Chiesa E, Pisani S, Genta I, Modena T, Bruni G, Brambilla CM, Benazzo M, Conti B. Evaluation of process parameters for fiber alignment of electrospun tubular nanofibrous matrices: a DoE approach; 2020.
[10] Maksimcuka J, Obata A, Sampson WW, Blanc R, Gao C, Withers PJ, et al. X-ray tomographic imaging of tensile deformation modes of electrospun biodegradable polyester fibres. Front Mater 2017;4:43.
[11] Stylianopoulos T, Kokonou M, Michael S, Tryfonos A, Rebholz C, Odysseos AD, et al. Tensile mechanical properties and hydraulic permeabilities of electrospun cellulose acetate fiber meshes. J Biomed Mater Res B Appl Biomater 2012;100(8):2222–30.
[12] Chen Y, Pan F, Guo Z, Liu B, Zhang J. Stiffness threshold of randomly distributed carbon nanotube networks. J Mech Phys Solids 2015;84:395–423.
[13] Zhang M, Chen Y, Chiang F-P, Gouma PI, Wang L. Modeling the Large Deformation and Microstructure Evolution of Nonwoven Polymer Fiber Networks. J Appl Mech 2019;86(1):011010.
[14] Yin Y, Xiong J. Finite element analysis of electrospun nanofibrous mats under biaxial tension. Nanomaterials 2018;8(5):348.
[15] Ban E, Barocas VH, Shephard MS, Picu CR. Effect of fiber crimp on the elasticity of random fiber networks with and without embedding matrices. J Appl Mech 2016;83(4):041008.
[16] Carleton JB, D'Amore A, Feaver KR, Rodin GJ, Sacks MS. Geometric characterization and simulation of planar layered elastomeric fibrous biomaterials. Acta Biomater 2015;12:93–101.
[17] Islam M, Tudryn GJ, Picu CR. Microstructure modeling of random composites with cylindrical inclusions having high volume fraction and broad aspect ratio distribution. Comput Mater Sci 2016;125:309–18.
[18] Picu RC. Mechanics of random fiber networks-a review. Soft Matter 2011;7(15):6768–85.
[19] Caballero DE, Montini-Ballarin F, Gimenez JM, Urquiza SA. Multiscale constitutive model with progressive recruitment for nanofibrous scaffolds. J Mech Behav Biomed Mater 2019;98:225–34.
[20] Peng Y, Deng K. Study on the mechanical properties of the novel Sn–Bi/Graphene nanocomposite by finite element simulation. J Alloys Compd 2015;625:44–51.
[21] Arash B, Wang Q, Liew KM. Wave propagation in graphene sheets with nonlocal elastic theory via finite element formulation. Comput Methods Appl Mech Eng 2012;223:1–9.
[22] Domaschke S, Morel A, Kaufmann R, Hofmann J, Rossi RM, Mazza E, et al. Predicting the macroscopic response of electrospun membranes based on microstructure and single fibre properties. J Mech Behav Biomed Mater 2020:103634.
[23] Pan F, Chen Y, Qin Q. Stiffness thresholds of buckypapers under arbitrary loads. Mech Mater 2016;96:151–68.
[24] Tserpes KI, Silvestre N. Modeling of carbon nanotubes, graphene and their composites. Springer; 2014.
[25] Pai CL, Boyce MC, Rutledge GC. On the importance of fiber curvature to the elastic moduli of electrospun nonwoven fiber meshes. Polymer 2011;52(26):6126–33.
[26] Silberstein MN, Pai CL, Rutledge GC, Boyce MC. Elastic-plastic behavior of non-woven fibrous mats. J Mech Phys Solids 2012;60(2):295–318.
[27] Yin Y, Pan Z, Xiong J. A tensile constitutive relationship and a finite element model of electrospun nanofibrous mats. Nanomaterials 2018;8(1):29.
[28] Zündel M, Mazza E, Ehret AE. A 2.5 D approach to the mechanics of electrospun fibre mats. Soft Matter 2017;13(37):6407–21.
[29] Domaschke S, Zündel M, Mazza E, Ehret AE. A 3D computational model of electrospun networks and its application to inform a reduced modelling approach. Int J Solids Struct 2019;158:76–89.
[30] Liu Y, Dzenis Y. Explicit 3D finite-element model of continuous nanofibre networks. Micro Nano Lett. 2016;11(11):727–30.
[31] Chen N, Silberstein M. Determination of bond strengths in non-woven fabrics: a combined experimental and computational approach. Exp Mech 2018;58(2):343–55.
[32] Negi V, Picu R. Mechanical behavior of nonwoven non-crosslinked fibrous mats with adhesion and friction. Soft Matter 2019;15(29):5951–64.
[33] Kallmes O, Corte H. The structure of paper, I. The statistical geometry of an ideal two dimensional fiber network. Tappi J 1960;43(9):737–52.
[34] González C, Llorca J. Stiffness of a curved beam subjected to axial load and large displacements. Int J Solids Struct 2005;42(5–6):1537–45.